



# Investigation of advanced laser-MAG tandem hybrid welding for joining gap-flawed thin sheet metal parts

S. Egerland<sup>1</sup> · H. Staufer<sup>1</sup> · M. Ruehrnoessl<sup>1</sup> · M. Schorn<sup>1</sup>

Received: 24 August 2016 / Accepted: 15 November 2017 / Published online: 18 December 2017  
© International Institute of Welding 2017

## Abstract

Decreasing wall thickness and part tolerances, e.g. gaps, adversely affect welding productivity. This paper is concerned with advanced laser-metal active gas (MAG) tandem hybrid welding (LTHW) providing a novel wire feeding concept and adjusting welding power by variable wire electrode diameters. 1.2- and 1.0-mm-diameter wires were used, respectively, for leading and trailing arc and were supplied to the process at the same feed rate. Given the experimental conditions, i.e. used for joining deliberately gap-flawed low wall thickness and small flange sheet metal lap joints, it was found that this novel LTHW concept is able to safely meet industrial requirements. The laser beam warrants for adequate fusion whilst the MAG-tandem process safely bridges the gap prepared. The results achieved are discussed and application perspectives derived focusing on technological aspects rather than on purely scientific considerations.

**Keywords** MAG tandem welding · Laser-MAG tandem hybrid welding · Lap joint welding

## 1 Introduction

Single-wire metal active gas (MAG) at increased travel speeds can cause imperfections, e.g. undercutting. A second wire electrode, trailing the first one, is suitable to eliminate defects and raise productivity [1, 2]. As early presented by Hackl [3], pulse synchronisation in pulsed metal inert gas tandem (MIG-T) welding can additionally stabilise process conditions. Nonetheless, different authors [4–9] claimed that controlling a comparatively higher number of process parameters as well as inappropriate weld torch design can negatively affect joint quality and efficiency.

Hedegård et al. [4]; Andersson et al. [5] and Motta and Dudra [6] have investigated variable contact tube inclination and wire electrode clearance. Goecke et al. [7] have recommended ‘adjustable’ electrodes and pulsed arc synchronisation to improve weld bead control. Andersson et al. could find a close relationship between parent material composition and electrode clearance and stated that the contact tube inclination

should allow to completely merge both arcs to act in a common process zone and minimising process instabilities.

Chen et al. [10]; Scotti et al. [11] and Ueyama et al. [12, 13] have studied arc interference and phase synchronisation as recommended, e.g. by Hackl [3]. Ueyama [14] for ferrous metals considers synchronisation with low delay times as an appropriate means to achieve high travel speed and mitigate arc interference. Scotti et al. whereas, for mild steel, have revealed the benefits of phase synchronisation depending on the mean transition current and assessed ‘*non-pulsing*’ power supplies capable of obtaining high-quality welds. Finally, Schnick et al. [15] have numerically modelled the effects of shielding gas composition on arc interference phenomena in pulsed MAG-T and reported that increasing CO<sub>2</sub> contents adversely affect arc stability.

Coupling an electric tungsten inert gas (TIG) welding arc with a laser beam is suggested to have been firstly accomplished by Steen [16]—referred to as ‘arc augmented laser processing’. Combinations of TIG or plasma arc welding (PAW) and lasers are reported to be subject of experimental [17–23], theoretical [24], or both, experimental and hypothetical investigation [25]. Compared with the aforementioned processes, MAG + laser, i.e. laser-MAG hybrid welding (LHW), is frequently employed under industrial environmental conditions. The amount of LHW research is extensive but

---

Recommended for publication by Commission XII - Arc Welding Processes and Production Systems

✉ S. Egerland  
egerland.stephan@fronius.com

<sup>1</sup> FRONIUS International GmbH, 4600 Wels, Austria

comprehensive overview of process development and state of the art is supplied by Bagger and Olsen [26]; Casalino et al. [27] and Victor [28].

Valuable recommendations on applicable electrode inclination and work angles are given by Harris [29] who has extensively studied high-performance-pulsed MAG and LHW and could show that pulsed LHW can overcome weld defects (humping bead) even at higher weld travel speed levels.

Experimental investigations were carried out on the effects of weld parameter interaction [30–34] and LHW to cope with weld defects [35–37]. A number of researchers were also concerned with industrial LHW applications and the corresponding results [38–44].

Apart from commercial publications, just little research data is available in terms of coupling dual wire MAG (tandem welding) and lasers. Among those few studies known to the authors however, Reis et al. [45] have contributed essential work by accurately investigating this subject. The laser was found stabilising the arcs independently of applying phase synchronisation.

More recently Wei et al. [46] have setup and studied a ‘triple-heat-source’ welding system consisting of two independent single-wire weld torches and a centred laser beam. They found positive effects on weld pool movement whilst shifting the pulsed currents to each other. Staufer et al. [47] have developed a LTHW head involving two independently controlled power supplies connected and operated with a diode-pumped 8-kW disc laser. Increased productivity and improved process behaviour with tolerance-affected parts were reported as the benefits in using this system. Finally, Staufer and Egerland [48] combined three arcs and one laser beam to achieve a setup, industrially applicable and capable of significantly increasing weld travel speed or weld deposition rate when applied in flat position on advanced high-strength steels of greater wall thickness.

## 2 Objectives

Conventional pulsed MAG-tandem (MAG-T) welding has shown limitations in joining low wall thickness parts and simultaneously supplying high weld travel speed [49]. Assuming the laser is capable of stabilising the process [45], this investigation was primarily aiming at quantifying the physical LTHW boundaries in low wall thickness part application. Special focus was laid on reduced flange lap joints to adequately involve the most current industrial environment requirements. Decreasing the lower sheet flange width is evaluated important due to increasing parent material efficiency thus dropping operational cost. For example, Staufer [49] could show that using MAG-T welding for joining thin sheet automotive parts was in demand to

prepare flange widths  $\geq 8$  mm to avoid excessive penetration and comply with quality standards.

## 3 Experimental

### 3.1 Specimen preparation and weld trial conduction

Lap joints with varying gap widths have been produced. The experimental setup was involving sheet metals of thickness 1.8 and 3.0 mm. The gap width was chosen both nought<sup>1</sup> and 1.0 mm. Figure 1 pictures the specimen dimensions, particularly pointing out the reduced flange width of the lower sheet.

The parent material was grade S 355 J2 (EN 10025-1:2005-02). The filler material was G3Si 1 (EN ISO 14341:2008). According to both aforementioned standards, Table 1 plots the parent metal melting lot-, and filler metal chemical composition as well as the mechanical properties.

MAG shielding gas applied was 96Ar/4O<sub>2</sub> (EN ISO 14175:2008 - M22) and welding position was ‘PB’ (EN ISO 6947). Two samples were produced for each condition whilst the work angle was  $\sim 5^\circ$  and the drag angle  $\sim 20^\circ$ , Fig. 2. Additionally, inclining the parts  $\leq 10^\circ$  towards torch movement resulted in welding conducted in forehand technique.

Four uniaxial shear tensile test specimens and one macro-section were taken from each welded coupon to quantitatively assign gap effects to joint properties as to visually assess the penetration profile. Figure 3 schematically reveals specific details on welding torch to laser beam adjustment, whilst Fig. 4 shows the shear tensile test specimen geometry.

### 3.2 Welding system

A MIG/MAG tandem welding configuration consisting of two digital inverter power sources ‘FRONIUS TPS 5000’ equipped with appropriate peripheral components (cooling and wire feeding systems) and remote control units was used.

It needs particular mention at this stage that a novel wire feeding concept has been developed and firstly was applied in this study. That is, the wire electrodes were pulled from a drum employing a special feeding unit type ‘WF 25i Reel SA’ and were supplied to the LTHW head containing a tandem feeder roll motor, Fig. 5.

The advancement in this LTHW process approach is factual that the motor drives both wire electrodes at the same feed rate, consequently leading to beneficial effects, e.g. reduced hose package weight and volume. Synergic welding characteristics provided by the welding power source and corresponding to each wire diameter now allow to easily control welding power by using different wire diameters. Diameters 1.2- and 1.0-mm wire electrodes, respectively, were used in

<sup>1</sup> Equal to technically zero gap.

**Fig. 1** Weld specimen dimensions. (Note, all values depicted are in mm)

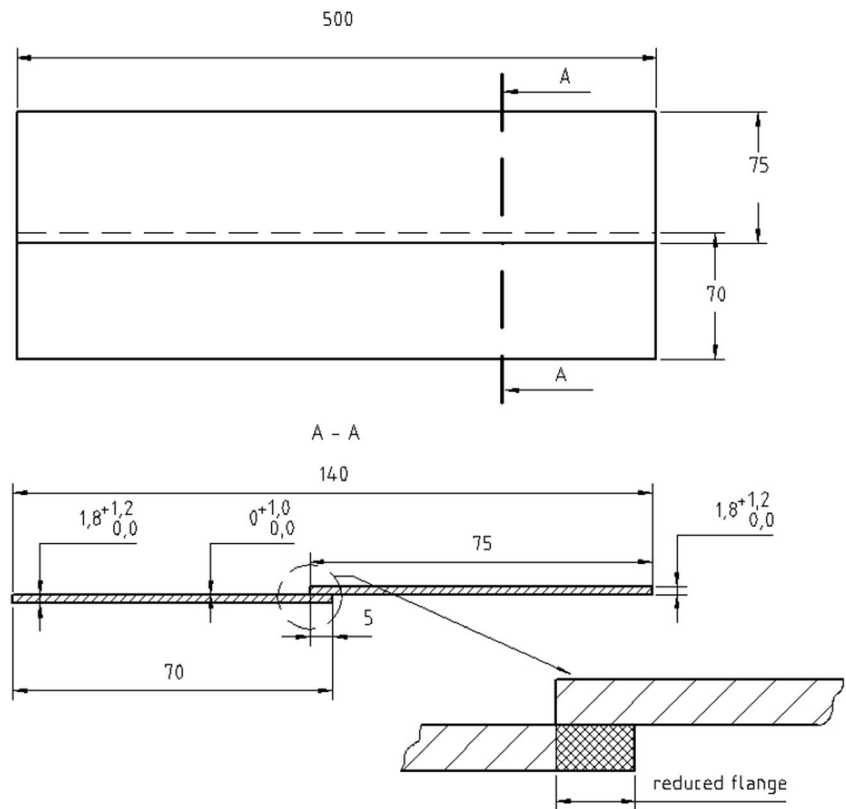
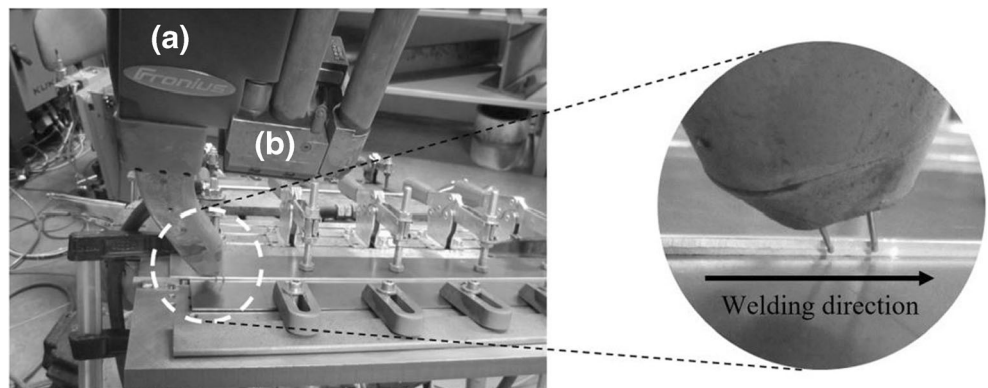


**Table 1** Chemical composition (weight percent) and mechanical properties of parent-and-filler material used

	C (%)	Si (%)	Mn (%)	P (%)	S (%)	Al (%)	N (%)	$R_{eH}$ (MPa)	$R_m$ (MPa)	A (%)
S 355 J2	0.164	0.212	1.460	0.013	0.0049	0.035	0.0043	410	549	24.1
G3Si1	0.07	0.77	1.30	0.013	0.013	–	–	440	540	30

$R_{eH}$  minimum yield strength,  $R_m$  tensile strength and A failure strain

**Fig. 2** Experimental jig with clamped specimen, LTHW torch (a) and laser head (b) with exploded view on torch inclination relative to workpiece



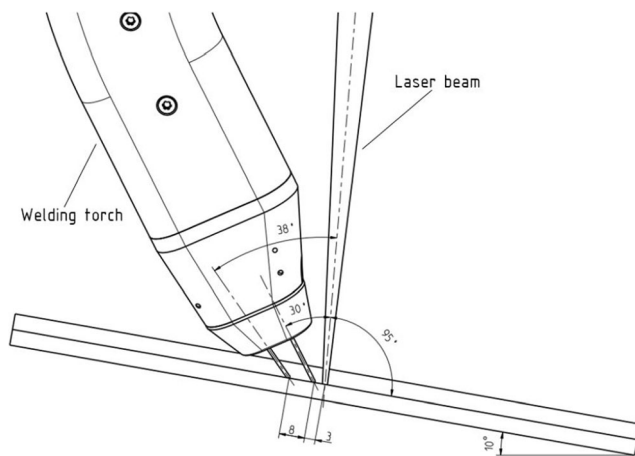


**Fig. 3** Schematic experimental adjustment of welding torch (wire electrode) and laser beam relative to specimen. (Note, bare numbers in the figure represent mm scale)

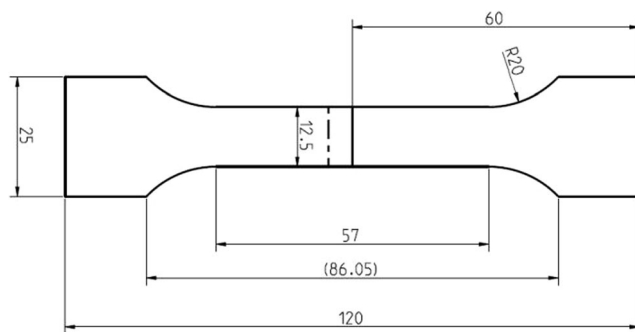


**Fig. 4** Uniaxial shear tensile test specimen geometry. (Note, all values depicted represent mm scale)

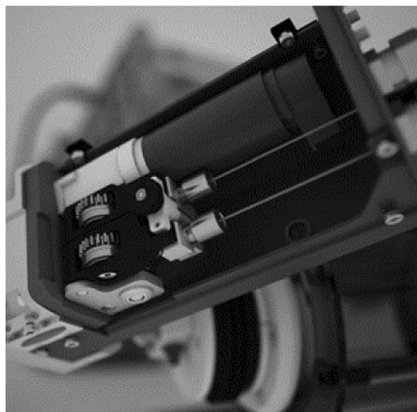


**Fig. 5** Wire feed concept designed for LTHW welding head

this investigation applying pulsed arc mode for leading and trailing arc because of using different synergic lines for both diameters that permitted to specifically adjust the welding power according to the experimental conditions and simultaneously to achieve maximum weld travel speeds for both specimen combinations. In this conjunction, the wire feed rate is set as a constant, as part of the appropriate synergic line stored in and made available by the welding power source employed. As regular with advanced welding equipment, the output current and voltage are adjusted then through the welding sequence corresponding to the specific synergic line (drooping and/or constant voltage characteristic), the part conditions and the consumables are used. Table 2 plots the most essential process parameters and additionally reveals the standard deviation for both current and voltage.

The developed welding head is applicable to  $\leq 6$ -kW laser power and  $2 \times 250$  A weld current (100% duty cycle). Lateral and longitudinal arc-laser adjustment of  $\pm 3$  and  $\pm 2$  mm, respectively, is feasible. A 6-axis articulated robot of KUKA ‘KR 30’ type was used for torch manipulation. The laser employed was a 10-kW diode-pumped TRUMPF ‘TRUDISK 10002’, and a type ‘BEO D35’ optics was installed in the focussing head. Involving a 200- $\mu$ m-diameter output optical fibre, adjusting a collimation length of 100 mm and a focal length of 300 mm resulted in a laser focal diameter of 0.6 mm.

## 4 Results

Because automotive parts, e.g. axle carriers, are regularly found flawed with gaps when supplied to welding under industrial environment, this investigation was seeking to derive threshold values for process conditions oriented at industrial specifications also used by Staufer [49]. Welding parameters were adjusted at zero gap conditions and subsequently used for 1.0-mm gap, i.e. the welding parameter sets were identical for gapless and gap-flawed series.

Proper root penetration with zero gap but simultaneously also bridging the 1.0-mm gap was achieved by increasing MAG welding and laser power. Also, as an important outcome, the process was found applicable to the reduced sheet

**Table 2** Welding parameters and standard deviation over all trials conducted

$t$ (mm)	$\bar{I}_{\text{lead}}$ (A)	$\bar{U}_{\text{lead}}$ (V)	$\bar{I}_{\text{trail}}$ (A)	$\bar{U}_{\text{trail}}$ (V)	$P_L$ (kW)	$V_{\text{wire}}$ (mmmin <sup>-1</sup> )	$V_{\text{weld}}$ (mmmin <sup>-1</sup> )
1.8	235 $\pm$ 1.13	22 $\pm$ 0.13	150 $\pm$ 1.09	21.5 $\pm$ 0.55	5.3	8.7	7.0
3.0	290 $\pm$ 1.21	23 $\pm$ 0.69	195 $\pm$ 1.12	22.5 $\pm$ 0.9	6.0	12.0	6.0

$t$  sheet thickness,  $\bar{I}$  mean welding current,  $\bar{U}$  mean welding voltage,  $P_L$  laser power,  $V_{\text{wire}}$  wire feed rate and  $V_{\text{weld}}$  weld travel speed



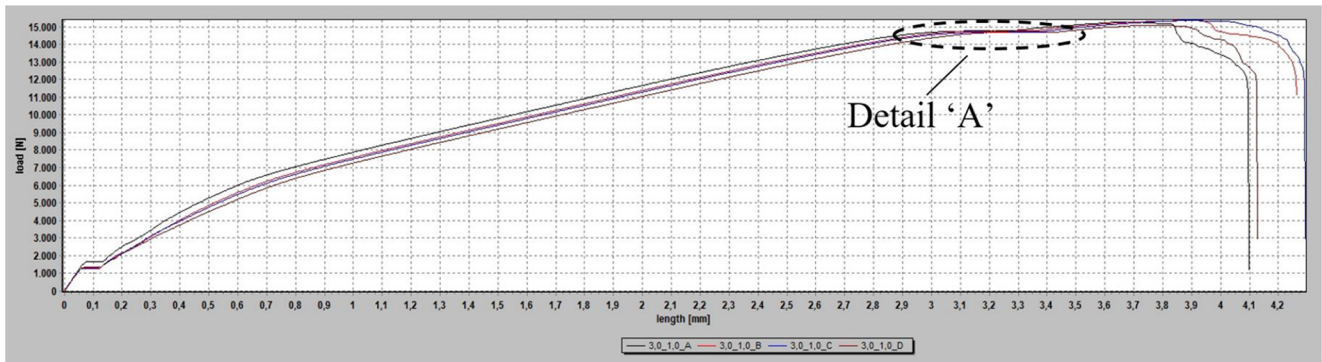


**Fig. 6** Original tensile test chart for sheet thickness 3.0 mm (gap flawed) plotting typical measured maximum load ( $F_{max}$ ) at theoretical peak value (point  $R_m$ ). (Note, ‘Detail A’ expanded in Fig. 7)

flange width of  $\leq 5$  mm although retaining adequate operational stability.

As both fracture in the parent and weld metal occurred, for the latter, the welded cross section under tensile load was practically unfeasible to precisely quantify. Hence, it proved

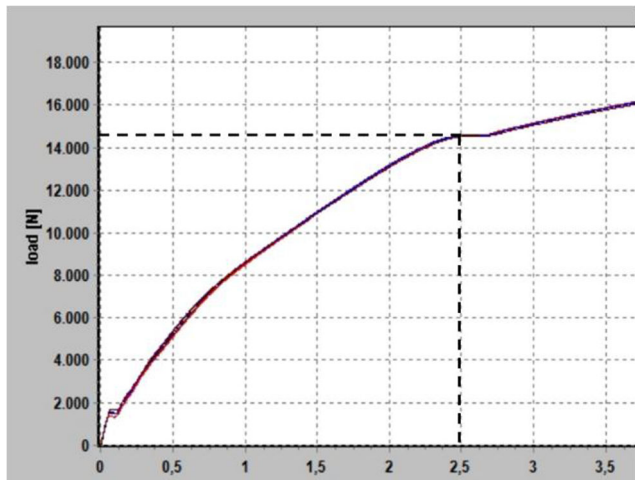
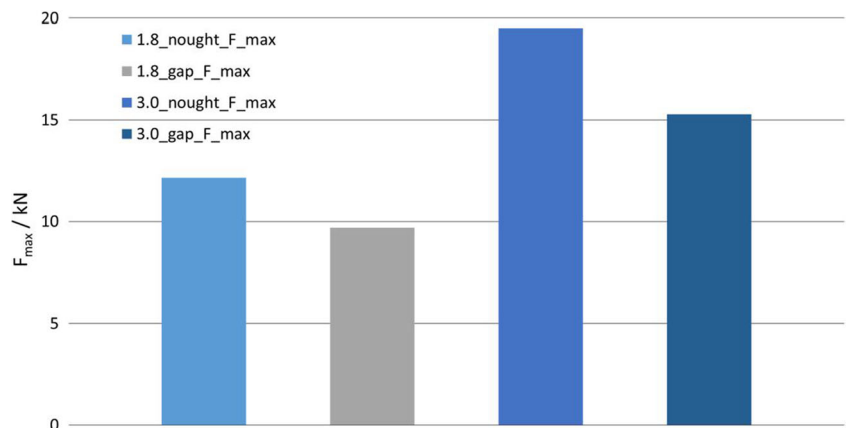


**Fig. 7** Detail ‘A’ showing the maximum load at theoretical tensile stress point  $R_m$ . (Note, horizontal axis depicts specimen elongation in mm)

**Fig. 8** Shear tensile test values for 1.8- and 3.0-mm-thickness both zero and 1.0-mm gap width.  $F_{max}$  force at maximum tensile load



impracticable to precisely define the weld joints’ mechanical properties, especially the tensile strength.

For the sake of comparison, i.e. to nonetheless obtain information on the weld joint mechanical properties, it was decided to derive and compare the maximum load ‘ $F_{max}$ ’ measured at the peak value in the stress-strain diagram (Fig. 6) actually representing the point of tensile strength. Figure 6 and Fig. 7 exemplarily draw tensile testing results obtained from a preliminary test series a gap-flawed 3.0-mm-thick specimen.

Finally, Fig. 8 depicts mean maximum load values taken for providing a more general understanding of the differences occurring through pulling the coupons. Figure 9 shows mean elongation and uniform elongation for all specimens tested.

Table 3 summarises the calculated values of all tested coupons for both thicknesses appropriately prepared with either 1.0-mm or zero gap.

Figure 10a–d for 3.0-mm-gauge samples shows transverse macro sections and hardness testing values. Interestingly, the peak values for the gap-flawed specimen were found  $\sim 50$  HV3 lower vs. that of the gap-free coupon.

Despite using both identical welding parameters and travel speed, the external bead appearance with the gap-prepared

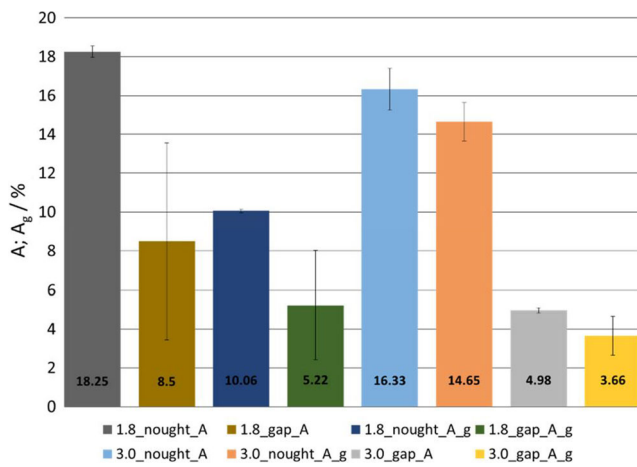


**Fig. 9** Elongation ( $A$ ) and uniform elongation ( $A_g$ ) for 1.8 and 3.0 mm both zero and 1.0-mm gap. (Note, error bars depict standard deviation)

**Table 3** Shear tensile test mean values for 1.8- and 3.0-mm wall thickness

Thickness (mm)	Gap (mm)	$F_{max}$ (kN)	$\bar{A}$ (%)	$\bar{A}_g$ (%)	Failure
1.8	1.0	9.685	8.5	5.22	Weld metal <sup>a</sup>
1.8	–	12.152	18.25	10.06	Parent metal
3.0	1.0	15.277	4.98	3.66	Weld metal
3.0	–	19.522	16.33	14.65	Parent metal

<sup>a</sup> One specimen failed in parent material

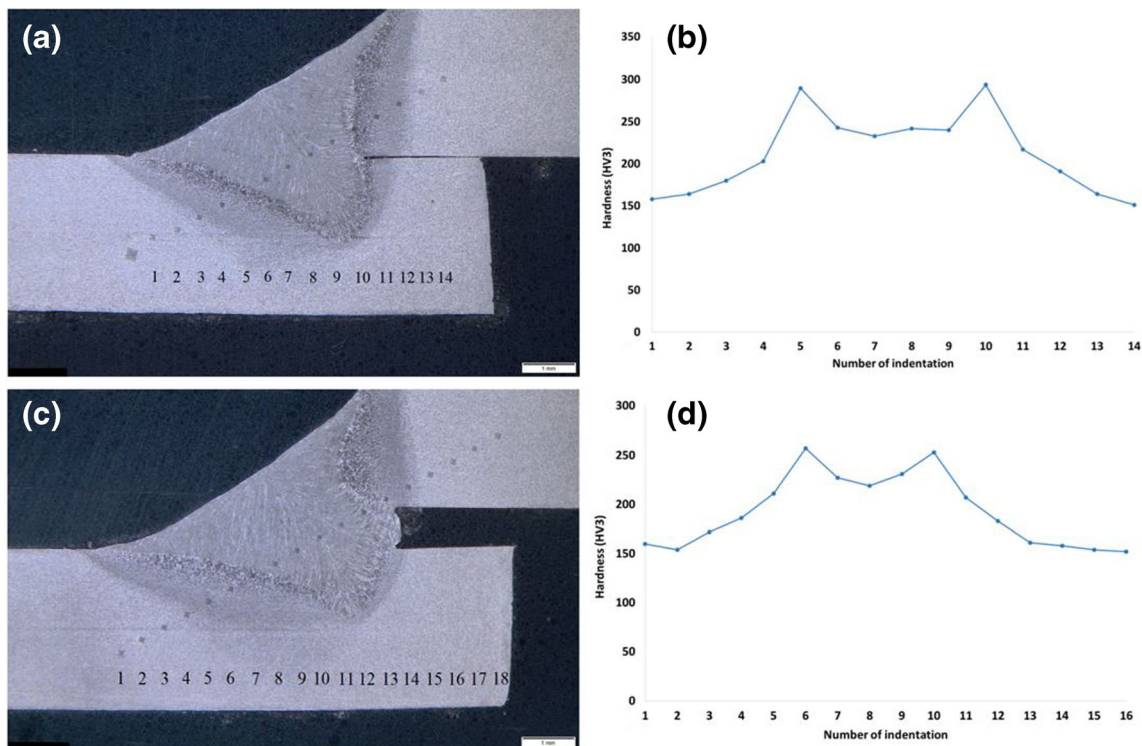
specimens was found fully complying with and due to reducing the flange width even outperforming industrial requirements [49]. Safe root penetration into the lower sheet with smooth notch-free transition between weld and parent metal was achievable and the joints remained free from excessive penetration.

Figure 11a–d shows the transverse macro sections for 1.8-mm wall thickness both for zero and 1.0-mm gap width; as well as the hardness profile for both specimen variants.

Figure 12 compares all hardness values evaluated. The weld deposit hardness was found generally higher vs. that of the parent material but lower than particularly the fusion line adjacent hardness. The 1.8-mm gap-free sample shows fusion line peak values approaching 350 HV3. The gap-flawed joints appear to interestingly reveal lower hardness peak values in general vs. those of the zero gap samples.

### 5 Discussion

We consider the feasibility of using two different wire electrode diameters fed at the same feed rates whilst simultaneously targeting at achieving maximum weld travel speeds as the technological value of this advanced LTHW principle.



**Fig. 10** Wall thickness 3.0 mm. **a** Transverse macro section and hardness profile of zero gap joint. **b** Corresponding zero gap hardness values. **c** Transverse macro section and hardness profile of 1-mm gap lap joint. **d** Corresponding hardness values

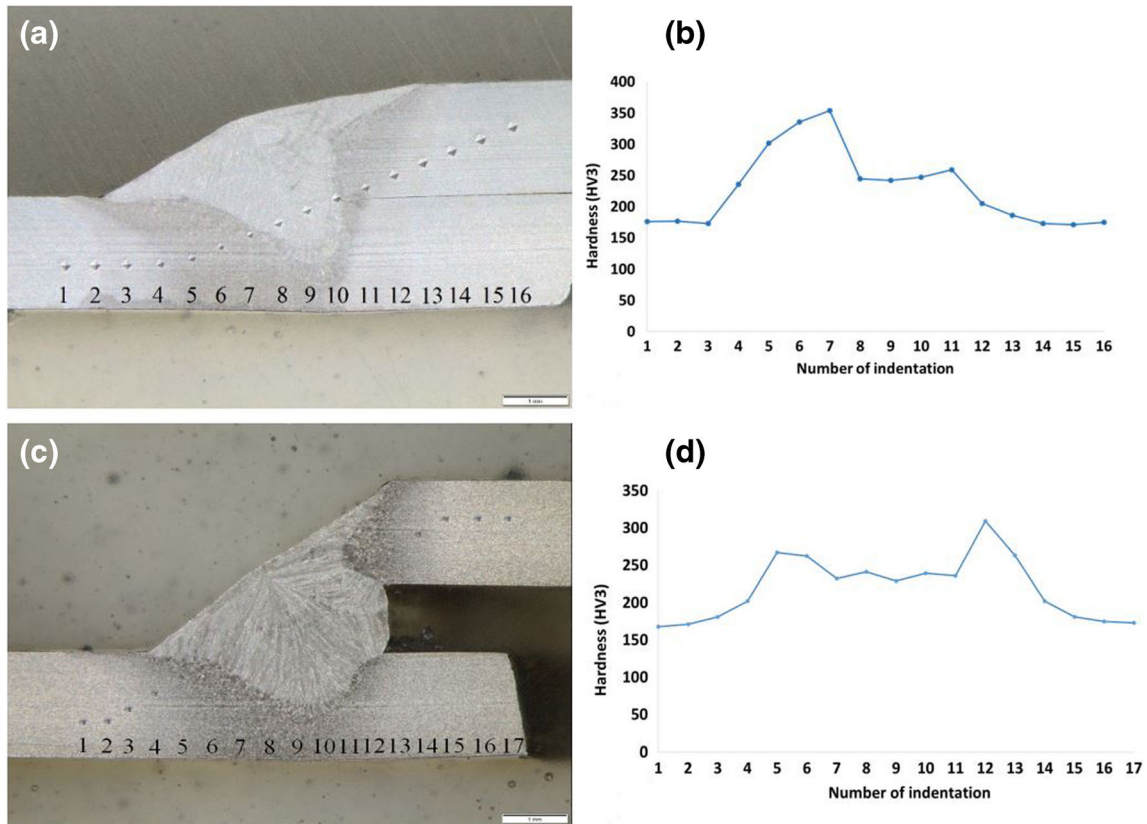


**Fig. 11** Wall thickness 1.8 mm. **a** Transverse macro section and hardness profile of zero gap lap joint. **b** Corresponding zero gap hardness values. **c** Transverse macro section and hardness profile of 1-mm gap lap joint. **d** Corresponding hardness values

In conjunction with both very high travel speed and considerable high dynamics in the weld pool, this was found degrading droplet detachment and general arc stability. That is, the leading arc plasma was found insufficiently extinguished whilst the trailing arc was already subject to ignition and arriving at the weld pool position previously covered by the leading wire arc.

Whilst we consider this as a general tendency even occurring with conventional high travel speed MAG-tandem

welding [3, 12, 13, 49], we have implemented the approach described and recommended by the same researchers, i.e. synchronising both arcs to obtain regular droplet detachment and improving process stability. However, it needs particular mention that this does not explicitly and generally contradict the results from Chen et al. [10] who were recommending to drastically reduce the phase difference between both weld current paths. That is, it was not yet tested whether the approach of Chen et al. may even outperform the process stability achieved

**Fig. 12** Hardness value overview of all tested specimens

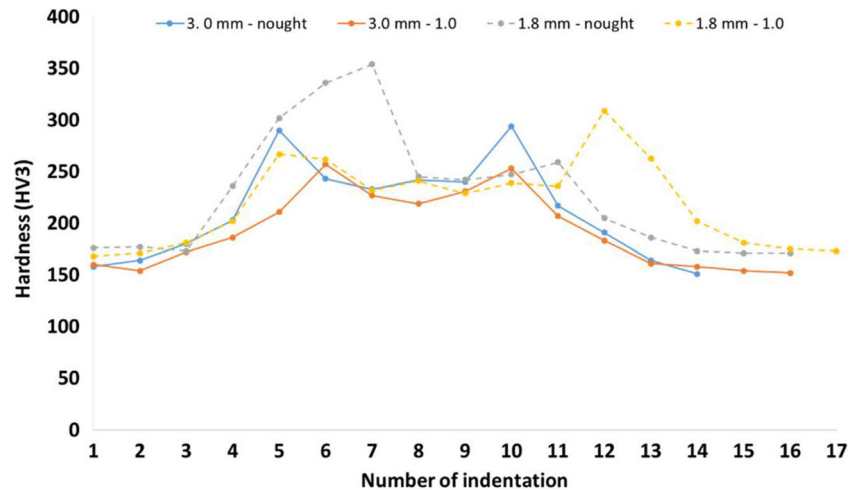






**Fig. 13** Welding voltage (lower values) and current (higher values) for both wire electrodes through applying advanced LTHW and using different wire electrode diameters at same wire feed rate. Upper portion shows leading arc; lower portion depicts trailing arc

by pulse synchronisation. Figure 13 shows the transient distribution of welding current and voltage for both wire electrodes after modifying the synergic characteristics used.

In general, we could find the laser stabilising the process, confirming thereby the results by Reis et al. [45]. This effect may also provide an explanation for the successful involvement of current and voltage synchronisation applied in our study. Compared with conventional pulsed MAG-tandem welding [49], the laser also permits for achieving superior travel speeds both with 1.8- and 3.0-mm sheet thickness. The increase of weld travel speed by the laser beam confirmed the assumptions of Stauer derived from his investigation in [49]. That is, weld travel speeds could be almost tripled vs. those of conventional MAG-tandem welding.

Since no excessive root penetration was found with both gauges investigated neither with zero nor 1.0-mm gap preparation, we suggest a reduction of the flange width of the lower sheet reliably applicable to industrial serial part production, e.g. axle carrier components of similar wall thickness and produced employing lap joint designs. We suppose the sound root bead fusion into the lower sheet also was beneficially assisted by adequately positioning the torch relative to the workpiece which would confirm the results by Harris [29] and dealing with the importance of this variable. The laser beam is permitted to produce reliable root penetration whilst the MAG-tandem process reliably fills the remainder joint cross section.

The uniaxial shear tensile test results confirmed our presumptions that the zero gap specimens, supposedly because of lower influence of bending in the joining area whilst pulling the coupons, approach the mechanical strength of the parent material. Consequently, the joint failure of all tested samples was revealed in the parent metal.

The lower sheets of the gap-flawed specimens were found significantly deformed which is presumably caused by side load effects due to asymmetric stress concentration around the gap area. In turn, all samples were observed failing in the weld metal. Although equivalent to the parent metal's yield strength, it should be interesting to further validate whether producing a greater bead reinforcement, i.e. increasing the weld deposition rate, might compensate for the loss in the joint's mechanical strength and elongation.

Quantifying the hardness for only one sample per combination prevents us from drawing a reasonable estimation for the variations found between flawless and gap-flawed specimens. However, it is nonetheless interesting that  $\sim 50$  HV3 lower hardness values were determined within the HAZ of the latter. Since found with both wall thicknesses, it is, in turn, suggested not arising through statistical error.

The hardness variations found between gap-free and gap-flawed coupons were part of microstructural investigation, limitedly conducted along with the mechanical tests and not further dealt with in this paper. Higher amounts of bainite in



the lower wall thickness part could be revealed which is suggested possibly caused by different heat conduction conditions. Consequently, we suppose the different hardness caused by heat dissipation variation between both specimen types, i.e. higher heat conduction with the unflawed specimens, may lead to an increase in the amount of microstructural constituents of higher hardness. However, further investigations may appear required to prove or understand this behaviour.

## 6 Conclusions

From the investigation conducted, we can summarise the following:

1. An advanced laser-MAG tandem hybrid welding (LTHW) process was developed applying different wire electrode diameters fed at the same wire feed rate but simultaneously varying welding power.
2. The novel LTHW variant was found reliably applicable to gap-flawed thin gauge sheet metal lap joint welding.
3. It was possible to almost triple the weld travel speed as to simultaneously reduce the lower sheet flange width by ~ 40% compared with conventional MAG-tandem welding.
4. Sound root fusion profiles with no excessive penetration into the lower sheet could be achieved with both wall thickness specimen series with zero gap and 1.0-mm gap width.
5. Pulsed current path synchronisation was found suitable to suppress arc interference and improve process stability.
6. The hardness peak values for the gap-flawed parts were ~ 50 HV3 lower vs. those of the zero gap specimens.
7. The uniaxial shear tensile test showed the gap-flawed specimens failing in the weld metal approaching the values as depicted in appropriate specifications.

**Acknowledgements** The authors are grateful to Mr. Philipp Doerner and Mr. Rick Grunwald both with Fronius International Research and Development for valuable assistance and conducting shear tensile and hardness testing. Special thanks shall be devoted to the peer reviewers for spending their valuable time, carefully reading the paper and raising meaningful comments and questions.

## References

1. Persson JA (1956) High-speed tandem arc working. USA Patent
2. Diez FM, Stump KS, Ludewig HW, Kilty AL, Robinson MM, Egland KM (2009) Dual wire welding torch and method. US Patent
3. Hackl H (1996) TIME twin—a novel double wire process for joining aluminium (IIW Doc. No. XII-1439-36). Paper presented at the C-XII Session of the 49th IIW Annual Assembly, Budapest
4. Hedegard J, Andersson J, Tolf E, Weman K, Lundin M (2004) Enhanced prospects for tandem-MIG/MAG welding. Paper presented at the C-XII Session of the 57th IIW Annual Assembly Osaka, Japan

5. Andersson J, Tolf E, Hedegard J (2006) The fundamental stability mechanism in TANDEM MIG/MAG welding, and how to perform implementation. In: Proceedings of the IIW International Conference. Quebec City, Canada. International Institute of Welding
6. Motta M, Dutra J (2006) Effects of the variables of the double wire MIG/MAG process with insulated potentials on the weld bead geometry. *Weld Int* 20(10):785–793. <https://doi.org/10.1533/weli.2006.20.10.785>
7. Goecke S, Hedegård J (2001) Tandem MIG/MAG welding. *Weld Rev* Published by Esab 56(2–3):24–28
8. Yudodibroto B, Hermans M, Richardson I (2006) The influence of pulse synchronisation on the process stability during TANDEM wire Arc welding. In: C-XII Session of the 59th IIW Annual Assembly 2006, Quebec City, Canada. vol IIW Doc. XII-1910-06
9. Yudodibroto BYB, Hermans MJA (2008) Richardson IM Process stability analysis during tandem wire arc welding. In: C-XII Session of the 59th IIW Annual Assembly 2006, Quebec City, Canada, 2008
10. Chen D, Chen M, Wu C (2015) Effects of phase difference on the behavior of arc and weld pool in tandem P-GMAW. *J Mater Process Technol* 225:45–55. <https://doi.org/10.1016/j.jmatprotec.2015.05.022>
11. Scotti A, Morais CO, Vilarinho LO (2006) The effect of out-of-phase pulsing on metal transfer in twin-wire GMA welding at high current level. *Weld J* 85(10):225s–230s
12. Ueyama T, Ohnawa T, Uezono T, Tanaka M, Ushio M, Nakata K (2005) Solution to problem of arc interruption and stable arc length control in tandem pulsed GMA welding—study of arc stability in tandem pulsed GMA welding (report 2). *Q J Jpn Weld Soc* 23(4): 526–535. <https://doi.org/10.2207/qjwvs.23.526>
13. Ueyama T, Ohnawa T, Yamazaki K, Tanaka M, Ushio M, Nakata K (2005) High-speed welding of steel sheets by the tandem pulsed gas metal arc welding system. *Trans JWRI* 34(1):11–18
14. Ueyama T (2010) Welding power sources. *Weld Int* 24(9):699–705. <https://doi.org/10.1080/09507111003655267>
15. Schnick M, Wilhelm G, Lohse M, Füssel U, Murphy AB (2011) Three-dimensional modelling of arc behaviour and gas shield quality in tandem gas-metal arc welding using anti-phase pulse synchronization. *J Phys D Appl Phys* 44(18):185205. <https://doi.org/10.1088/0022-3727/44/18/185205>
16. Steen WM (1980) Arc augmented laser processing of materials. *J Appl Phys D* 51(11):5636–5641. <https://doi.org/10.1063/1.327560>
17. Chen Y, Miao Y, Li L, Wu L (2008) Arc characteristics of laser-TIG double-side welding. *Sci Technol Weld Join* 13(5):438–444. <https://doi.org/10.1179/174329308X341861>
18. Zhiyong L, Srivatsan T, Yan L, Wenzhao Z (2013) Coupling of laser with plasma arc to facilitate hybrid welding of metallic materials: a review. *J Mater Eng* 22(2):384–395
19. Swanson P, Page C, Read E, Wu H (2007) Plasma augmented laser welding of 6 mm steel plate. *Sci Technol Weld Join* 12(2):153–160. <https://doi.org/10.1179/174329307X164283>
20. Liu L, Hao X, Song G (2006) A new laser-arc hybrid welding technique based on energy conservation. *Mater Trans* 47(6):1611–1614. <https://doi.org/10.2320/matertrans.47.1611>
21. Hu B, Den Ouden G (2005) Laser induced stabilisation of the welding arc. *Sci Technol Weld Join* 10(1):76–81. <https://doi.org/10.1179/174329305X29537>
22. Hu B, Den Ouden G (2005) Synergetic effects of hybrid laser/arc welding. *Sci Technol Weld Join* 10(4):427–431. <https://doi.org/10.1179/174329305X44170>
23. Suder W, Ganguly S, Williams S, Paradowska A, Colegrove P (2011) Comparison of joining efficiency and residual stresses in laser and laser hybrid welding. *Sci Technol Weld Join* 16(3):244–248. <https://doi.org/10.1179/1362171810Y.0000000020>

24. Ribic B, Rai R, DebRoy T (2008) Numerical simulation of heat transfer and fluid flow in GTA/laser hybrid welding. *Sci Technol Weld Join* 13(8):683–693. <https://doi.org/10.1179/136217108X356782>
25. Yoon S, Hwang J, Na S (2007) A study on the plasma-augmented laser welding for small-diameter STS tubes. *Int J Adv Manuf Technol* 32(11–12):1134–1143. <https://doi.org/10.1007/s00170-006-0436-3>
26. Bagger C, Olsen FO (2005) Review of laser hybrid welding. *J Laser Appl* 17(1):2–14. <https://doi.org/10.2351/1.1848532>
27. Casalino G, Dal Maso U, Angelastro A, Campanelli S (2010) Hybrid laser welding: a review. *DAAAM International Scientific Book* 38:413
28. Victor BM (2011) Hybrid laser arc welding. In: Lienert TS, Babu S, Acoff V (ed) *ASM handbook, Welding fundamentals and processes*, vol 6A. pp 321–328
29. Harris ID (2009) High-speed GMAW and laser GMAW hybrid welding of steel sheet. PhD-Thesis, Cranfield University, UK
30. Gao M, Zeng X, Hu Q (2006) Effects of welding parameters on melting energy of CO<sub>2</sub> laser-GMA hybrid welding. *Sci Technol Weld Join* 11(5):517–522. <https://doi.org/10.1179/174329306X148138>
31. Tusek J, Suban M (1999) Hybrid welding with arc and laser beam. *Sci Technol Weld Join* 4(5):308–311. <https://doi.org/10.1179/136217199101537923>
32. Zhang W, Hua X, Liao W, Li F, Wang M (2014) Behavior of the plasma characteristic and droplet transfer in CO<sub>2</sub> laser-GMAW-P hybrid welding. *Int J Adv Manuf Technol* 72(5–8):935–942. <https://doi.org/10.1007/s00170-014-5731-9>
33. El Rayes M, Walz C, Sepold G (2004) The influence of various hybrid welding parameters on bead geometry. *Weld J* 83(5):147–S
34. Xu W-j, Wu C-s, Zou D-g (2008) Predicting of bead undercut defects in high-speed gas metal arc welding (GMAW). *Front Mater Sci China* 2(4):402–408. <https://doi.org/10.1007/s11706-008-0065-x>
35. Kim Y-C, Hirohata M, Inose K (2014) Verification of possibility for controlling welding distortion generated by laser-arc hybrid welding. *Int J Steel Struct* 14(2):323–329. <https://doi.org/10.1007/s13296-014-2012-2>
36. Choi H, Farson D, Cho M (2006) Using a hybrid laser plus GMAW process for controlling the bead humping defect. *Weld J* 85(8):174–179
37. Engström H, Nilsson K, Flinkfeldt J, Nilsson T, Skirfors A, Gustavsson B (2001) Laser hybrid welding of high strength steels. In: *Proc. ICALEO*, pp 125–134
38. Graf T, Staufer H (2003) Laser-hybrid welding drives VW improvements. *Weld J* 82(1):42–48
39. Staufer H, Ruehmossel M, Miessbacher G (2003) Hybrid welding for the automotive industry. *Ind Laser Solut Manuf* 1:7–10
40. Matsusaka S, Uezono T, Tsumura T, Tanaka M, Watanabe T (2008) Laser-arc hybrid welding process of galvanized steel sheets. *Mater Sci Forum* 580–582:355–358
41. Kawahito Y, Mizutani M, Katayama S (2009) High quality welding of stainless steel with 10 kW high power fibre laser. *Sci Technol Weld Join* 14(4):288–294. <https://doi.org/10.1179/136217108X372531>
42. Kah P (2011) Usability of laser—arc hybrid welding processes in industrial applications. PhD-Thesis, Lappeenranta University of Technology, Lappeenranta, Finland
43. Ono M, Shinbo Y, Yoshitake A, Ohmura M (2002) Development of laser-arc hybrid welding. *NKK Technical Report-Japanese Edition* 70–74:8–12
44. Thomy C (2010) Gap tolerant laser GMA hybrid welding process for thin sheet materials. Paper presented at the C-XII Session of the 63rd IIW Annual Assembly, Istanbul, Turkey
45. Reis RP, Norrish J, Cuiuri D (2011) Preliminary evaluations on laser—tandem GMAW. *Weld World* 55(9–10):41–49. <https://doi.org/10.1007/BF03321319>
46. Wei H, Li H, Yang L, Gao Y, Ding X (2014) Arc characteristics and metal transfer process of hybrid laser double GMA welding. *Int J Adv Manuf Technol* 77(5–8):1019–1028
47. Staufer H (2010) Operation and visualisation of the laser hybrid twin welding process (IIW Doc. SG-212-1174-10, XII-2003-10, IV-1040-10). Paper presented at the C-IV/C-XII/SG-212 Joint Meeting of the 63rd IIW Annual Assembly, Istanbul, Turkey
48. Staufer H (2010) Three arc laser hybrid gas shielded metal arc welding—high-performance processes for joining high-strength steel pipes of greater wall thickness (IIW Doc. IV-1028-10). Paper presented at the C-IV Session of the 63rd IIW Annual Assembly, Istanbul, Turkey
49. Staufer H (2015) MAG-tandem welding of reduced flange automotive parts. Fronius International GmbH (unpublished work), Wels, Austria